

# **The regulation of intestinal bicarbonate secretion by marine teleost fish**

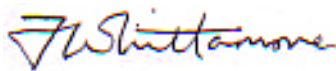
**Volume 1 (of 2)**

Submitted by Jonathan Mark Whittamore, to the University of Exeter as a thesis for the degree of Doctor of Philosophy in Biological Sciences in December 2008.

This thesis is available for library use on the understanding that it is copyright material and that no quotation from the thesis may be published without proper acknowledgement.

I certify that all material in this thesis which is not my own work has been identified and that no material previously submitted and approved for the award to a degree by this or any other University.

Signature



Date **10<sup>th</sup> December 2008**

**Acknowledgements**

I would like to extend my sincere gratitude to supervisor Dr. Rod Wilson for all his encouragement, advice and for offering the benefits of his knowledge and experience over many enjoyable discussions throughout the course of this project. Likewise, I am also very grateful to friend and colleague Dr. Chris Cooper, with whom it has been a pleasure to work these past few years. In addition, I would like to thank Jan Shears and Margaret Grapes for their excellent technical assistance. Thank you also to Dr Martin Grosell at the University of Miami for the opportunity to visit his laboratory, as well as Josi Taylor, Janet Genz and the rest of his research group for their wonderful hospitality. I would also like to thank the many members (past and present) of the Ecotoxicology and Ecophysiology research group here at the School of Biosciences. Finally, I wish to express my deep gratitude to my family for their encouragement and support throughout.

This work was funded by a studentship from the Biotechnology and Biological Sciences Research Council (BBSRC).

## **Abstract**

In seawater, drinking is a fundamental part of the osmoregulatory strategy for teleost fish, and presents a unique challenge. The intestine has an established role in osmoregulation, and its ability to effectively absorb fluid from imbibed seawater is crucial to compensating for water losses to the surrounding hyperosmotic environment. Alongside solute-linked water transport (driven by NaCl cotransport), intestinal bicarbonate ( $\text{HCO}_3^-$ ) secretion also benefits fluid absorption directly (*via* apical  $\text{Cl}/\text{HCO}_3^-$  exchange), and indirectly through the formation of calcium carbonate ( $\text{CaCO}_3$ ) thus removing the osmotic influence of  $\text{Ca}^{2+}$  within the gut fluid. For the European flounder (*Platichthys flesus*), elevated luminal  $\text{Ca}^{2+}$  has proven to be a specific, potent stimulator of  $\text{HCO}_3^-$  secretion both *in vitro* and *in vivo* where these actions are presumably modulated by an extracellular  $\text{Ca}^{2+}$ -sensing receptor (CaR). The focus of this work was to learn more about how intestinal  $\text{HCO}_3^-$  secretion is regulated, the role of  $\text{Ca}^{2+}$ , and more specifically the CaR. To achieve this, *in vitro* 'gut sac' experiments investigated how luminal  $\text{Ca}^{2+}$  influenced  $\text{HCO}_3^-$  secretion, and associated ion and fluid transport. Contrary to expectation, increasing  $\text{Ca}^{2+}$  from 5 to 20 mM did not stimulate  $\text{HCO}_3^-$  secretion. In an attempt to elucidate the role of  $\text{CaCO}_3$  precipitation in fluid absorption, and further explore the physiological implications of  $\text{HCO}_3^-$  secretion, the intestine was perfused *in vivo* with salines containing varying concentrations of  $\text{Ca}^{2+}$  (10, 40 and 90 mM). The production and secretion of  $\text{HCO}_3^-$ , in addition to  $\text{CaCO}_3$  formation increased accordingly with  $\text{Ca}^{2+}$ , and was associated with a dramatic 25 % rise in the fraction of fluid absorbed by the gut. Additional *in vitro* experiments, utilising the Ussing chamber, helped establish some of the characteristics of intestinal  $\text{HCO}_3^-$  secretion by the euryhaline killifish (*Fundulus heteroclitus*), but was unresponsive to elevated mucosal  $\text{Ca}^{2+}$ . Further attempts to potentiate the activity of the CaR, and application of the receptor agonists gadolinium ( $\text{Gd}^{3+}$ ) and neomycin, failed to produce responses consistent with the effect of  $\text{Ca}^{2+}$  observed previously, either *in vitro* or *in vivo*. With no evidence supporting a direct role for an extracellular, intestinal CaR in  $\text{HCO}_3^-$  secretion it was argued that secretion would be principally regulated by two factors, the ability of the epithelia to generate high levels of intracellular  $\text{HCO}_3^-$  and the rate of  $\text{CaCO}_3$  formation.

## Contents

### List of Figures

<b>List of Tables</b>	13
<b>List of Plates</b>	14
<b>Chapter 1 – Introduction</b>	15
<b>1. The challenge of life in the sea</b>	17
1.1 Osmoconformity	19
1.2 Osmoregulation	19
<b>2. The osmoregulatory strategy of marine teleost fish</b>	20
2.1 Drinking	20
2.2 Processing imbibed seawater	21
2.2.1 The gastrointestinal tract	21
2.2.2 Oesophagus	23
2.2.3 Intestine	23
2.2.4 Gills	24
2.2.5 Kidney and urinary bladder	25
<b>3. The role of the intestine in osmoregulation</b>	27
3.1 Anatomical structure	27
3.2 Ion transport	29
3.3 Fluid transport	31
3.3.1 Aquaporins	32
3.3.2 Is there active fluid transport?	33
3.3.3 Calcium carbonate precipitation	34
<b>4. Regulation of intestinal HCO<sub>3</sub><sup>-</sup> secretion</b>	35
4.1 Osmoregulation and intestinal HCO <sub>3</sub> <sup>-</sup> secretion	35
4.2 The calcium-sensing receptor (CaR)	36
4.2.1 Structure and diversity	36
4.2.2 Agonists and modulators	37
4.2.3 Tissue distribution and functions	39
4.2.4 Roles in health and disease	39
4.3 The CaR in teleosts	41
4.3.1 Distribution and proposed functions	41
4.3.2 A role for the CaR in marine teleost osmoregulation	42
<b>5. Project overview</b>	44
<b>Chapter 2 – Measuring fluid transport <i>in vitro</i>: Gravimetric method versus non-absorbable marker</b>	45
<b>1. Summary</b>	46
<b>2. Introduction</b>	46
2.1 Development of the gut sac as an <i>in vitro</i> technique	47
2.2 Measuring fluid transport by gut sacs	49
2.3 Non-absorbable volume markers	50
2.4 Using PEG as a marker	52
2.5 Aims and objectives	52
<b>3. Materials and Methods</b>	53
3.1 Experimental animals	53

3.2	Saline design and composition	54
3.3	General experimental approach	56
3.4	Measuring fluid transport in gut sacs: Gravimetric versus PEG	57
3.5	Entry of PEG into the serosal saline	59
3.6	Removal of PEG from gut sacs	60
3.7	Distribution of PEG within gut sacs	61
3.8	Interaction of PEG with the mucosal layer	63
3.9	PEG as a volume marker	63
3.10	The performance of unlabelled PEG + [ <sup>14</sup> C] PEG in gut sacs	64
3.11	Data presentation and statistical analysis	65
<b>4.</b>	<b>Results</b>	65
4.1	Measuring fluid transport in gut sacs: Gravimetric versus [ <sup>14</sup> C] PEG	65
4.2	Entry of PEG into the serosal saline	67
4.3	Removal of PEG from gut sacs	68
4.4	Distribution of PEG within gut sacs	68
4.5	Interaction of PEG with the mucosal layer	68
4.6	PEG as an indicator of volume	69
4.7	Using unlabelled PEG as a 'carrier' for [ <sup>14</sup> C] PEG in gut sacs	71
<b>5.</b>	<b>Discussion</b>	74
5.1	The appearance of [ <sup>14</sup> C] PEG in the serosal saline	74
5.2	Calculating the residual fluid volume in gut sacs	76
5.3	Does [ <sup>14</sup> C] PEG distribute evenly within the gut sac?	77
5.4	Interactions between PEG and the mucosal layer	79
5.4.1	Chemistry of PEG and the mucus layer	79
5.4.2	Interactions of PEG with the mucus layer from gut sacs	80
5.5	Adsorption of PEG	82
5.5.1	Using unlabelled PEG as a 'carrier'	82
5.6	Conclusion	83
<b>Chapter 3 – Evaluating the paired gut sac technique for measurement of ion and fluid transport <i>in vitro</i></b>		84
<b>1.</b>	<b>Summary</b>	85
<b>2.</b>	<b>Introduction</b>	86
2.1	Assessing the viability of the intestine <i>in vitro</i>	87
2.2	The energetic requirements of the intestine	88
2.3	The functional capacity of the intestine <i>in vitro</i>	89
2.4	Glucose and glutamine as metabolic fuels	90
2.5	Aims and objectives	91
<b>3.</b>	<b>Materials and Methods</b>	92
3.1	Experimental animals	92
3.2	Saline design and composition	92
3.3	Concentrations of glucose and glutamine	94
3.4	Pre-incubation period	94
3.5	Functional viability of the gut sac preparation	95
3.6	Hydrostatic pressure effects	96

3.7	Sample analysis and ion flux calculations	97
3.8	Data presentation and statistical analysis	98
<b>4.</b>	<b>Results</b>	99
4.1	Pre-incubation period	99
4.2	Regional differences in ion and fluid transport	99
4.3	Stability of ion and fluid transport over time	101
<b>5.</b>	<b>Discussion</b>	103
5.1	Pre-incubation period	103
5.2	Regional differences in ion and fluid transport	104
5.3	The stimulation of ion and fluid transport by glucose and glutamine	106
5.3.1	Adaptation of the intestine in response to luminal nutrients	108
5.4	The effect of metabolism on intestinal HCO <sub>3</sub> <sup>-</sup> secretion	109
5.4.1	Was the supply of oxygen limiting?	110
5.4.2	Anaerobic energy production by the intestine	110
5.5	Conclusions and perspectives	111
<b>Chapter 4 - The regulation of bicarbonate secretion by the marine teleost intestine <i>in vitro</i></b>		113
<b>1.</b>	<b>Summary</b>	114
<b>2.</b>	<b>Introduction</b>	115
2.1	The gastrointestinal tract in marine teleost osmoregulation	115
2.2	The role of intestinal HCO <sub>3</sub> <sup>-</sup> secretion and precipitation in osmoregulation	116
2.3	Mechanism and source of HCO <sub>3</sub> <sup>-</sup> secretion	116
2.3.1	The role of anion exchange	116
2.3.2	Source of HCO <sub>3</sub> <sup>-</sup>	117
2.3.3	Basolateral H <sup>+</sup> secretion	119
2.4	Regulation of HCO <sub>3</sub> <sup>-</sup> secretion	120
2.5	Aims and objectives	122
<b>3.</b>	<b>Materials and Methods</b>	123
3.1	Experimental animals	123
3.2	Saline design and composition	123
3.3	Experiment #1 – Effect of Ca <sup>2+</sup> on HCO <sub>3</sub> <sup>-</sup> secretion	125
3.4	Experiment #2 – The role of serosal CO <sub>2</sub>	125
3.4.1	Effect of 2 % CO <sub>2</sub> on the composition of the serosal saline	125
3.5	Experiment #3 – The effects of Ca <sup>2+</sup> on basolateral H <sup>+</sup> secretion	127
3.6	Sample analysis and flux calculations	128
3.7	Data presentation and statistical analysis	129
<b>4.</b>	<b>Results</b>	129
4.1	Experiment #1 – Effect of Ca <sup>2+</sup> on HCO <sub>3</sub> <sup>-</sup> secretion	129
4.2	Experiment #2 – The role of serosal CO <sub>2</sub>	131
4.2.1	Effect of 2 % CO <sub>2</sub> on the composition of the serosal saline	132
4.3	Experiment #3 – The effects of Ca <sup>2+</sup> on basolateral H <sup>+</sup> secretion	132
<b>5.</b>	<b>Discussion</b>	136

5.1	Experiment #1 – Effect of $\text{Ca}^{2+}$ on $\text{HCO}_3^-$ secretion	136
	5.1.1 Is $\text{HCO}_3^-$ secretion impaired when using the gut sac preparation?	136
	5.1.2 Influence of the mucus layer and $\text{CaCO}_3$ precipitation	138
	5.1.3 Is $\text{CaCO}_3$ precipitation likely to take place in gut sacs?	141
5.2	Experiment #2 – The role of serosal $\text{CO}_2$	141
	5.2.1 Effect of 2 % $\text{CO}_2$ on the composition of the serosal saline	143
	5.2.2 Can $\text{CO}_2$ regulate $\text{NaCl}$ transport in the flounder intestine?	144
5.3	Experiment #3 – The effects of $\text{Ca}^{2+}$ on basolateral $\text{H}^+$ secretion	147
	5.3.1 The role of endogenous $\text{CO}_2$ in luminal $\text{HCO}_3^-$ secretion	147
	5.3.2 Net flux of acid-base equivalents <i>in vitro</i>	149
	5.3.3 The effect of elevated mucosal $\text{Ca}^{2+}$ on basolateral $\text{H}^+$ secretion	150
	5.3.4 The regulation of intestinal ion and fluid transport by $\text{Ca}^{2+}$	152

## List of figures

	Page
<b>Figure 1.1:</b> A comparative illustration of the basic organisational plan of the vertebrate digestive system.	22
<b>Figure 1.2:</b> The general layout of the vertebrate intestine.	28
<b>Figure 1.3:</b> A model of the principal cellular ion and fluid transport pathways across the marine teleost intestinal epithelia.	31
<b>Figure 1.4:</b> A schematic representation of the principal topological features of the CaR protein.	38
<b>Figure 2.1A:</b> An illustration of the elaborate circulation system for the perfusion of a section of rat intestine.	48
<b>Figure 2.1B:</b> A diagram showing the preparation of an everted gut sac, alongside a photograph of an everted gut sac from the hamster.	48
<b>Figure 2.2:</b> A comparison of the mean rates of intestinal fluid transport measured simultaneously by the gravimetric method and [ <sup>14</sup> C] PEG using gut sacs from the intestines of the European flounder and rainbow trout.	66
<b>Figure 2.3:</b> The time course of fluid transport by gut sacs from the flounder intestine based on [ <sup>14</sup> C] PEG.	69
<b>Figure 2.4:</b> The mean proportions of [ <sup>14</sup> C] PEG initially injected into gut sacs that were found associated with the mucosal layer at the start of an incubation and 2 hours later.	70
<b>Figure 2.5:</b> The relationship between the mean volume change to a fixed volume of mucosal saline following the addition of different volumes of deionised water.	71
<b>Figure 2.6:</b> A comparison of the mean rates of intestine fluid transport measured simultaneously by the gravimetric method and [ <sup>14</sup> C] PEG, using unlabelled PEG as a carrier, by gut sacs from the European flounder intestine.	72
<b>Figure 2.7:</b> The mean proportion of [ <sup>14</sup> C] PEG initially injected into gut sacs that was found to be associated with the mucosal layer at the start of an incubation, and 2 hours later at the end, using unlabelled PEG as a carrier.	73
<b>Figure 2.8:</b> The time course of net water fluxes by an isolated segment of everted eel intestine.	78
<b>Figure 3.1:</b> The time course of fluid transport by gut sacs from the flounder	100



intestine.

**Figure 3.2:** The mean net transport rates of  $\text{Na}^+$ ,  $\text{Cl}^-$  and  $\text{HCO}_3^-$ , alongside net fluid transport by gut sacs from the anterior, mid and posterior segments of the flounder intestine in the presence of varying amounts of glucose and glutamine. 101

**Figure 3.3:** The mean net transport rates of  $\text{Na}^+$ ,  $\text{Cl}^-$  and  $\text{HCO}_3^-$ , alongside net fluid transport by gut sacs from the intestine of the European flounder in the presence of varying amounts of glucose and glutamine. 102

**Figure 4.1:** An example of the typical titration curves obtained following the titration of the initial and final samples of the serosal saline. 128

**Figure 4.2:** The mean net fluxes of  $\text{Na}^+$ ,  $\text{Cl}^-$  and  $\text{HCO}_3^-$ , alongside net fluid transport by gut sacs from the flounder intestine under control conditions, and in response to a 15 mM increase in mucosal  $\text{Ca}^{2+}$  concentration. 130

**Figure 4.3:** The mean net fluxes of  $\text{Na}^+$ ,  $\text{Cl}^-$  and  $\text{HCO}_3^-$ , alongside net fluid transport by gut sacs made from the anterior, mid and posterior sections of the flounder intestine in relation to changes in mucosal  $\text{Ca}^{2+}$  and serosal  $\text{CO}_2$ . 131

**Figure 4.4:** The mean net fluxes of  $\text{Na}^+$  and  $\text{Cl}^-$  alongside net fluid transport by gut sacs made from the anterior, mid and posterior sections of the flounder intestine in response to elevated mucosal  $\text{Ca}^{2+}$ , and in the absence of serosal  $\text{HCO}_3^-/\text{CO}_2$ . 134

**Figure 4.5:** The mean net flux of  $\text{HCO}_3^-$  into the mucosal saline in relation to the opposite acidic efflux detected in the serosal saline by gut sacs made from the anterior, mid and posterior sections of the flounder intestine in response to elevated mucosal  $\text{Ca}^{2+}$  and in the absence of serosal  $\text{HCO}_3^-/\text{CO}_2$ . 135

**Figure 4.6:** The mean concentration of  $\text{HCO}_3^-$  measured in the mucosal saline of gut sacs from the European flounder after being incubated for 1, 2 and 8 hours under control, *in vivo*-like conditions. 138

**Figure 4.7:** A proposed model of the processes involved in  $\text{NaCl}$  and fluid absorption by the proximal intestine of the European flounder in response to elevated intracellular  $\text{CO}_2$  derived from either metabolism or external sources. 145

**Figure 4.8:** The relationship between net apical  $\text{HCO}_3^-$  secretion and net basolateral  $\text{H}^+$  secretion by gut sacs from the anterior, mid and posterior sections of the flounder intestine. 149

## List of Tables

	Page
<b>Table 1.1:</b> The typical ionic composition and osmolality of seawater compared with the blood plasma of a number of fish species representing the classes Agnatha, Chondrichthyes and infra-class Teleostei.	18
<b>Table 2.1:</b> The salts used in the composition of the mucosal and serosal salines.	55
<b>Table 2.2:</b> The mean proportion of [ <sup>14</sup> C] PEG detected in various compartments of gut sacs (serosal saline, rinses of the sac lumen and mucosal layer), from the flounder and rainbow trout.	67
<b>Table 2.3:</b> The change in activity of [ <sup>14</sup> C] PEG after being aliquoted from a working stock of mucosal saline into clean, dry tubes made from a range of different materials.	70

<b>Table 2.4:</b> The mean mass of the mucosal layer removed from the anterior, mid and posterior gut sacs at the beginning, and at the end of an incubation.	81
<b>Table 3.1:</b> The inorganic salts used to compose the mucosal and serosal salines.	93
<b>Table 3.2:</b> Calculations of the mean tissue density of various regions of the flounder intestine.	106
<b>Table 4.1:</b> The inorganic salts used in the composition of the mucosal and serosal salines employed in the following experiments.	124
<b>Table 4.2:</b> The mean measured pH and total CO <sub>2</sub> from samples taken at regular intervals from serosal saline being continuously gassed over 3 hours with either 0.5 % CO <sub>2</sub> or 2 % CO <sub>2</sub> .	133
<b>Table 4.3:</b> A comparison of mean luminal HCO <sub>3</sub> <sup>-</sup> secretion by gut sacs from the flounder under serosal conditions with 0.5 % CO <sub>2</sub> and 8 mM HCO <sub>3</sub> <sup>-</sup> present in the serosal saline and 100 % O <sub>2</sub> , 0 mM HCO <sub>3</sub> <sup>-</sup> .	148

## List of Plates

<b>Plate 2.1:</b> A typical gut sac made from the intestine of the European flounder.	Page 56
---	------------

**The regulation of intestinal bicarbonate secretion  
by marine teleost fish**

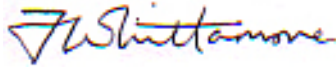
**Volume 2 (of 2)**

Submitted by Jonathan Mark Whittamore, to the University of Exeter as a thesis for the degree of Doctor of Philosophy in Biological Sciences in December 2008.

This thesis is available for library use on the understanding that it is copyright material and that no quotation from the thesis may be published without proper acknowledgement.

I certify that all material in this thesis which is not my own work has been identified and that no material previously submitted and approved for the award to a degree by this or any other University.

Signature



Date **10<sup>th</sup> December 2008**

## Contents

	Page
<b>List of Figures</b>	163
<b>List of Tables</b>	167
<b>List of Plates</b>	169
<b>Chapter 5 – The role of intestinal HCO<sub>3</sub><sup>-</sup> production, secretion and precipitation in fluid absorption and Ca<sup>2+</sup> homeostasis by a marine teleost.</b>	170
<b>1. Summary</b>	171
<b>2. Introduction</b>	172
2.1 A historical perspective on fluid transport	172
2.2 The mechanism of intestinal fluid transport in teleosts	174
2.3 The role of intestinal HCO <sub>3</sub> <sup>-</sup> secretion and precipitation in fluid transport	175
2.4 The role of CaCO <sub>3</sub> precipitation in Ca <sup>2+</sup> homeostasis	177
<b>3. Materials and Methods</b>	178
3.1 Experimental animals	178
3.2 <i>In vivo</i> surgical procedures	179
3.2.1 Cannulation of the caudal blood vessel	179
3.2.2 Fitting the intestinal perfusion and stomach drain catheters	181
3.2.3 Fitting the rectal catheter	181
3.3 Saline composition and experimental design	183
3.4 Intestinal perfusion	185

3.5	Sampling and analytical techniques	186
3.6	Calculations	187
3.7	Data presentation and statistical analysis	189
<b>4.</b>	<b>Results</b>	189
4.1	Bicarbonate production and excretion	189
4.2	Rectal fluid osmolality	191
4.3	Fluid transport	191
4.4	Fate of the divalent cations ( $\text{Ca}^{2+}$ and $\text{Mg}^{2+}$ )	193
4.5	Blood chemistry	195
<b>5.</b>	<b>Discussion</b>	197
5.1	The influence of luminal osmotic pressure	197
5.2	Solute-linked water transport	199
5.3	A role for apical $\text{Cl}^-/\text{HCO}_3^-$ exchange	200
5.4	Endogenous $\text{CO}_2$ hydration	201
5.4.1	Intestinal $\text{H}^+$ production and systemic acid-base balance	203
5.5	The contribution of $\text{HCO}_3^-$ production, secretion and precipitation to fluid absorption	204
5.5.1	A hypo- or hyper-osmotic absorbate?	206
5.5.2	A role for $\text{CO}_2$ in intestinal fluid absorption	207
5.6	The role of intestinal $\text{CaCO}_3$ precipitation in $\text{Ca}^{2+}$ homeostasis	211
5.6.1	Calculating the rate of intestinal $\text{Ca}^{2+}$ absorption	212
5.6.2	Regulating intestinal $\text{Ca}^{2+}$ transport	212
5.6.3	Summary	213
<b>Chapter 6 – The regulation of intestinal <math>\text{HCO}_3^-</math> secretion by the seawater-adapted killifish (<i>Fundulus heteroclitus</i> L.)</b>		215
<b>1.</b>	<b>Summary</b>	216
<b>2.</b>	<b>Introduction</b>	217
2.1	The Ussing chamber	217
2.2	Measuring $\text{HCO}_3^-$ secretion in the Ussing chamber	218
2.3	The euryhaline killifish	220
2.4	Does ionic strength influence intestinal $\text{HCO}_3^-$ secretion?	221
2.5	Aims and objectives	222
<b>3.</b>	<b>Materials and Methods</b>	222
3.1	Experimental animals	222
3.2	General experimental protocol	223
3.3	Stimulation of $\text{HCO}_3^-$ secretion by $\text{Ca}^{2+}$	225
3.4	Is $\text{HCO}_3^-$ secretion modulated by ionic strength and/or osmolality?	226
3.4.1	Effects of mucosal hyper-osmolality	226
3.4.2	Source of $\text{HCO}_3^-$ secretion	227
3.4.3	Basolateral $\text{H}^+$ secretion in relation to mucosal osmotic pressure	227
3.4.4	Mediation of apical $\text{HCO}_3^-$ and $\text{H}^+$ secretion	228
3.5	Buffer capacity of mannitol and sucrose	228

3.6	Saline design and composition	229
3.7	Calculations	229
3.8	Data presentation and statistics	231
<b>4.</b>	<b>Results</b>	231
4.1	Stimulation of HCO <sub>3</sub> <sup>-</sup> secretion by Ca <sup>2+</sup>	231
4.2	Is HCO <sub>3</sub> <sup>-</sup> secretion modulated by ionic strength and/or osmolality?	233
4.2.1	Effects of mucosal hyper-osmolality	237
4.2.2	Source of HCO <sub>3</sub> <sup>-</sup> secretion	241
4.2.3	Basolateral H <sup>+</sup> secretion in relation to mucosal osmotic pressure	243
4.2.4	Mediation of apical HCO <sub>3</sub> <sup>-</sup> and H <sup>+</sup> secretion	245
4.3	Buffer capacity of mannitol and sucrose	247
<b>5.</b>	<b>Discussion</b>	248
5.1	Stimulation of HCO <sub>3</sub> <sup>-</sup> secretion by Ca <sup>2+</sup>	248
5.2	Is HCO <sub>3</sub> <sup>-</sup> secretion modulated by ionic strength and/or osmolality?	248
5.2.1	Other effects on epithelial ion transport	250
5.2.2	A role for the CFTR?	251
5.3	Effects of mucosal hyperosmolality and the role of cell volume regulation	252
5.3.1	The source of HCO <sub>3</sub> <sup>-</sup>	253
5.3.2	Basolateral H <sup>+</sup> secretion	254
5.4	The response of the killifish intestine to mucosal hyperosmolality	255
5.4.1	Mediation of apical HCO <sub>3</sub> <sup>-</sup> and H <sup>+</sup> secretion	257
5.4.2	The mechanism of HCO <sub>3</sub> <sup>-</sup> secretion <i>in vitro</i>	258
5.4.3	Physiological significance	259
<b>Chapter 7 – Is there a role for the calcium-sensing receptor in the regulation of ion and fluid transport by the marine teleost intestine?</b>		261
<b>1.</b>	<b>Summary</b>	262
<b>2.</b>	<b>Introduction</b>	263
2.1	Calcium homeostasis	264
2.2	Salinity sensor	265
2.3	Intestinal ion and fluid transport	266
2.4	Epithelial barrier function	267
2.5	Digestion and nutrient sensing	268
2.6	Aims and objectives	269
<b>3.</b>	<b>Materials and Methods</b>	270
3.1	Experimental animals	270
3.2	<i>In vitro</i> experiments	271
3.2.1	General experimental approach	271
3.2.2	Is HCO <sub>3</sub> <sup>-</sup> secretion modulated by ionic strength and/or	271

	osmolality?	
	3.2.3 Applying agonists of the calcium-sensing receptor (CaR)	271
	3.2.4 Saline design and composition	274
3.3	<i>In vivo</i> experiments	274
	3.3.1 Experimental approach and salines	274
3.4	Data presentation and analysis	274
<b>4.</b>	<b>Results</b>	276
4.1	The influence of saline composition on HCO <sub>3</sub> <sup>-</sup> secretion	276
	4.1.1 Regular mucosal saline	276
	4.1.2 Reduced ionic strength mucosal saline	277
	4.1.3 Reduced osmolality saline	278
4.2	The effect of calcium-sensing receptor (CaR) agonists on ion and fluid transport <i>in vitro</i>	278
	4.2.1 Gadolinium (Gd <sup>3+</sup> )	278
	4.2.2 Neomycin	281
4.3	The effect of calcium-sensing receptor (CaR) agonists on ion and fluid transport <i>in vivo</i>	282
	4.3.1 Bicarbonate production and excretion	282
	4.3.2 Fluid transport	283
<b>5.</b>	<b>Discussion</b>	284
5.1	Why is HCO <sub>3</sub> <sup>-</sup> secretion in gut sacs NOT stimulated by Ca <sup>2+</sup> ?	285
	5.1.1 Thermodynamic considerations for HCO <sub>3</sub> <sup>-</sup> secretion <i>in vitro</i>	286
	5.1.2 The driving forces for Cl <sup>-</sup> /HCO <sub>3</sub> <sup>-</sup> exchange	287
	5.1.3 The electrochemical potential ( $\Delta\mu$ )	288
	5.1.4 Is diffusion of CO <sub>2</sub> into the epithelial cell limited?	290
	5.1.5 Additional barriers to Cl <sup>-</sup> /HCO <sub>3</sub> <sup>-</sup> exchange in gut sacs	291
	5.1.6 Summary	292
5.2	The role of CaCO <sub>3</sub> production in HCO <sub>3</sub> <sup>-</sup> secretion <i>in vivo</i>	292
	5.2.1 Is a CaR required for HCO <sub>3</sub> <sup>-</sup> secretion <i>in vivo</i> ?	293
5.3	A role for the CaR <i>in vitro</i>	297
5.4	Is Cl <sup>-</sup> /HCO <sub>3</sub> <sup>-</sup> exchange a driving force for fluid transport <i>in vitro</i> ?	298
	<b>Chapter 8 – General discussion</b>	304
<b>1.</b>	<b>The Ca<sup>2+</sup>-sensing receptor and regulation of intestinal HCO<sub>3</sub><sup>-</sup> secretion</b>	305
<b>2.</b>	<b>Fluid absorption by the marine teleost intestine</b>	309
	2.1 Absorbing a hyperosmotic fluid	309
	2.2 The influence of basolateral H <sup>+</sup> secretion	309
	2.3 Absorption of an iso-osmotic fluid	310
	2.4 Further implications of intestinal H <sup>+</sup> production	312
<b>3.</b>	<b>Concluding remarks</b>	313
	<b>References</b>	314



## List of figures

	Page
<b>Figure 5.1:</b> A simple illustration of solute-coupled fluid absorption across an epithelia.	174
<b>Figure 5.2:</b> The mean net production and excretion of $\text{HCO}_3^-$ equivalents by the intestine of the flounder.	190
<b>Figure 5.3:</b> The mean osmolality of the perfusate entering the intestine and the voided rectal fluid from the flounder following perfusion of the intestine.	192
<b>Figure 5.4:</b> The mean proportion of fluid absorbed by the flounder intestine.	193
<b>Figure 5.5:</b> The mean amounts of $\text{Ca}^{2+}$ and $\text{Mg}^{2+}$ presented to, and recovered from the intestine and rectal catheters of the flounder following perfusion of the intestine.	194
<b>Figure 5.6:</b> The relationship between the net fluxes of $\text{Na}^+$ and $\text{Cl}^-$ , and the corresponding rate of fluid absorption by the intestine of the flounder.	199
<b>Figure 5.7:</b> A comparison of the mean net fluxes of cations and anions by the	201

intestine of the flounder.	
<b>Figure 5.8:</b> The relationship between the total rate of $\text{HCO}_3^-$ secretion and ‘missing cation’ absorbed by the intestine of the flounder.	202
<b>Figure 5.9:</b> The relationship between the net titratable acid flux via non-intestinal routes into the surrounding seawater and the ‘missing cation’ absorbed by the intestine of the flounder.	204
<b>Figure 5.10:</b> The relationship between the rate of fluid transport predicted to be associated with $\text{HCO}_3^-$ production, secretion and precipitation, and the total rate of $\text{HCO}_3^-$ secretion by the intestine of the flounder.	205
<b>Figure 5.11:</b> A model illustrating the potential pathway for the removal of excess $\text{H}^+$ arising from intracellular $\text{CO}_2$ hydration.	208
<b>Figure 5.12:</b> The relationship between calculated osmolality of the absorbed fluid, minus the contribution of $\text{H}^+$ , and the measured total rate of $\text{HCO}_3^-$ secretion by the intestine of the flounder.	210
<b>Figure 6.1:</b> A) A schematic drawing of a circulating Ussing chamber. B) A plan view of the two halves of the tissue mount inserted between the two half chambers.	219
<b>Figure 6.2:</b> Measurements of transepithelial potential, transepithelial conductance and $\text{HCO}_3^-$ secretion from the isolated anterior intestine of the killifish following the addition of $\text{CaCl}_2$ or $\text{MgCl}_2$ to the mucosal saline.	232
<b>Figure 6.3:</b> Measurements of transepithelial potential, transepithelial conductance and $\text{HCO}_3^-$ secretion from the isolated anterior intestine of the killifish following the addition of $\text{CaCl}_2$ or $\text{MgCl}_2$ to the ‘reduced ionic strength’ mucosal saline.	234
<b>Figure 6.4:</b> Measurements of transepithelial potential, transepithelial conductance and $\text{HCO}_3^-$ secretion from the killifish intestine following the addition of $\text{CaCl}_2$ or $\text{MgCl}_2$ to the ‘reduced osmolality’ mucosal saline.	236
<b>Figure 6.5:</b> Measurements of transepithelial potential, transepithelial conductance and $\text{HCO}_3^-$ secretion from the isolated anterior intestine of <i>F. heteroclitus</i> following the addition of mannitol or sucrose.	238
<b>Figure 6.6:</b> The pH of the mucosal saline logged over the course of an experiment.	240
<b>Figure 6.7:</b> Measurements of transepithelial potential, transepithelial conductance and $\text{HCO}_3^-$ secretion from the killifish intestine after replacing the serosal saline, followed by the addition of sucrose to the mucosal saline.	242
<b>Figure 6.8:</b> Measurements of transepithelial potential, transepithelial conductance and the serosal secretion of acidic equivalents from the isolated anterior intestine of the killifish following the addition of mannitol or sucrose.	244

<b>Figure 6.9:</b> Measurements of transepithelial potential, transepithelial conductance and $\text{HCO}_3^-$ secretion from the isolated anterior intestine of the killifish following the application of DIDS and amiloride.	246
<b>Figure 6.10:</b> The amount of base required to increase the pH of the reduced osmolality mucosal saline in order to determine any changes in buffer capacity following the addition of either mannitol or sucrose.	247
<b>Figure 6.11:</b> Measurements of transepithelial potential, transepithelial conductance and $\text{HCO}_3^-$ secretion from the killifish intestine responding to an increase in mucosal osmolarity.	256
<b>Figure 7.1:</b> The mean net fluxes of $\text{Na}^+$ , $\text{Cl}^-$ and $\text{HCO}_3^-$ alongside net fluid transport by gut sacs from the flounder intestine under control conditions, and in response to a 15 mM increase in mucosal $\text{Ca}^{2+}$ concentration using the ‘regular’ mucosal saline.	276
<b>Figure 7.2:</b> The mean net fluxes of $\text{Na}^+$ , $\text{Cl}^-$ and $\text{HCO}_3^-$ , alongside net fluid transport by gut sacs from the flounder intestine under control conditions, and in response to a 15 mM increase in mucosal $\text{Ca}^{2+}$ concentration using the ‘reduced ionic strength’ mucosal saline.	277
<b>Figure 7.3:</b> The mean net fluxes of $\text{Na}^+$ , $\text{Cl}^-$ and $\text{HCO}_3^-$ , alongside net fluid transport by gut sacs from the flounder intestine under control conditions, and in response to a 15 mM increase in mucosal $\text{Ca}^{2+}$ concentration using the ‘reduced osmolality’ mucosal saline.	279
<b>Figure 7.4:</b> The mean net fluxes of $\text{Na}^+$ , $\text{Cl}^-$ and $\text{HCO}_3^-$ , alongside net fluid transport by gut sacs from the flounder intestine under control conditions, and in response to $\text{Gd}^{3+}$ .	280
<b>Figure 7.5:</b> The mean net fluxes of $\text{Na}^+$ , $\text{Cl}^-$ and $\text{HCO}_3^-$ , alongside net fluid transport by gut sacs from the flounder intestine under control conditions, and in response to neomycin.	281
<b>Figure 7.6:</b> The mean net production and excretion of $\text{HCO}_3^-$ equivalents by the intestine of the flounder perfused with salines containing the CaR agonists $\text{Gd}^{3+}$ or neomycin.	282
<b>Figure 7.7:</b> The mean proportion of fluid absorbed by the flounder intestine following perfusion with salines containing the CaR agonists $\text{Gd}^{3+}$ or neomycin.	284
<b>Figure 7.8:</b> (A) Mucus globules exiting from the goblet cell, demonstrating how $\text{Ca}^{2+}$ becomes concentrated in the mucus. (B) Needle-like $\text{Ca}^{2+}$ -rich crystals are clearly visible within the overlying mucus layer. (C) A simple schematic diagram	294

illustrating the potential role for  $\text{CaCO}_3$  crystallisation in  $\text{HCO}_3^-$  secretion.

**Figure 7.9:** The mean net  $\text{Na}^+$  and  $\text{Cl}^-$  fluxes by the intestine of the flounder perfused with salines containing the CaR agonists  $\text{Gd}^{3+}$  and neomycin. 296

**Figure 7.10:** The net fluxes of  $\text{Cl}^-$  and  $\text{HCO}_3^-$  in relation to net fluid transport 299

using the overall mean values pooled from anterior, mid and posterior gut sacs.

**Figure 7.11:** The relationships between net sodium flux, net fluid transport rate, and the concentration of  $\text{Na}^+$  in the mucosal saline with gut sacs from the European flounder 302

**Figure 8.1:** The concentration of  $\text{HCO}_3^-$  in the anterior, mid, posterior and rectal fluids sampled from the intestine of the Gulf toadfish (*Opsanus beta*) acclimated to a range of salinities from 2.5 to 70 ppt. 307

## List of Tables

<b>Table 5.1:</b> The inorganic salts used in the composition of the <i>in vivo</i> perfusion salines employed by the present study.	186
<b>Table 5.2:</b> The mean values for measurements of pH, TCO <sub>2</sub> and calculated HCO <sub>3</sub> <sup>-</sup> equivalents measured in rectal fluid samples from the flounder following perfusion of the intestine.	191
<b>Table 5.3:</b> A summary of the various acid-base and osmoregulatory parameters measured on whole blood (pH) and plasma (Osmolality, TCO <sub>2</sub> , Na <sup>+</sup> , Cl <sup>-</sup> , K <sup>+</sup> , Ca <sup>2+</sup> and Mg <sup>2+</sup> ) as part of the daily blood sampling routine during perfusion of the flounder intestine.	196
<b>Table 5.4:</b> The ionic composition of the rectal fluid following intestinal perfusion.	198
<b>Table 6.1:</b> The composition of the mucosal and serosal salines.	230
<b>Table 6.2:</b> A comparison of the ionic composition of the ‘regular’ mucosal saline used in the present study with the mucosal saline used by Wilson <i>et al.</i> (2002).	249
<b>Table 7.1:</b> The inorganic salts and additional solutes used in the composition of the mucosal and serosal salines.	273
<b>Table 7.2:</b> The inorganic salts used in the composition of the <i>in vivo</i> perfusion salines.	275
<b>Table 7.3:</b> The mean values of pH, TCO <sub>2</sub> and calculated HCO <sub>3</sub> <sup>-</sup> equivalents measured in rectal fluid samples from the flounder following perfusion of the intestine with salines containing the CaR agonists, Gd <sup>3+</sup> and neomycin.	283
<b>Table 7.4:</b> The electrochemical potentials of Cl <sup>-</sup> and HCO <sub>3</sub> <sup>-</sup> across the intestinal epithelia of the European flounder at the beginning and the end of <i>in vitro</i> gut sac experiments.	288
<b>Table 7.5:</b> A comparison of the electrochemical potentials for Na <sup>+</sup> , K <sup>+</sup> and Cl <sup>-</sup> as well as apical NaCl co-transport, for the ‘regular’ mucosal saline and ‘reduced ionic strength’ mucosal saline used with gut sacs from the intestine of the European flounder	301
<b>Table 8.1:</b> The reduction in osmotic pressure of fluid absorbed by the teleost intestine <i>in vitro</i> , following the buffering of absorbed H <sup>+</sup> by the extracellular fluid.	311

## List of Plates

	Page
<b>Plate 5.1:</b> A flounder under anaesthesia on the wet table the gills being irrigated <i>via</i> the mouth and implantation of the blood catheter.	180
<b>Plate 5.2:</b> Insertion of the stomach drain catheter and intestinal perfusion catheter.	182
<b>Plate 5.3:</b> Fitting the rectal catheter.	184
<b>Plate 6.1:</b> The Ussing chamber set up with pH stat.	225